High-sensitivity investigation of low-lying dipole strengths in ^{120}Sn

M. Müscher,[1,*] J. Wilhelmy,[1] R. Massarczyk,[2] R. Schwengner,[3] M. Grieger,[3] J. Isaak,[4] A. R. Junghans,[3] T. Kögler,[3,5,6] F. Ludwig,[3] D. Savran,[7] D. Symochko,[4] M. P. Takács,[3,†] M. Tamkas ,[7,‡] A. Wagner,[3] and A. Zilges[1]

[1]*Universität zu Köln, Institut für Kernphysik, 50937 Köln, Germany*

[2]*Los Alamos National Laboratory, Los Alamos, New Mexico 87545, USA*

[3]*Institut für Strahlenphysik, Helmholtz-Zentrum Dresden-Rossendorf, 01328 Dresden, Germany*

[4]*Institut für Kernphysik, Technische Universität Darmstadt, 64289 Darmstadt, Germany*

[5]*OncoRay - National Center for Radiation Research in Oncology, Faculty of Medicine and University Hospital Carl Gustav Carus, Technische Universität Dresden, Helmholtz-Zentrum Dresden-Rossendorf, 01309 Dresden, Germany*

[6]*Institut für Radioonkologie - OncoRay, Helmholtz-Zentrum Dresden-Rossendorf, 01328 Dresden, Germany*

[7]*GSI Helmholtzzentrum für Schwerionenforschung GmbH, 64291 Darmstadt, Germany*

(Received 22 April 2020; accepted 2 July 2020; published 21 July 2020)

Background: The term Pygmy Dipole Resonance (PDR) denotes an accumulation of electric dipole excitations below and around the neutron separation threshold. It may be important, e.g., for the nucleosynthesis of heavy nuclei or the symmetry energy in the Equation of State (EoS). For a deeper understanding of the PDR, systematic studies are essential.

Purpose: The tin isotopic chain is a well-suited candidate to investigate the systematics of the PDR, and the (γ, γ') reactions on ^{112,116,120,124}Sn have already been measured in experiments using bremsstrahlung. It was claimed that the extracted electric dipole transition strengths of these isotopes increase with increasing neutron-to-proton ratio with the exception of ^{120}Sn. Furthermore, previous results from elastic photon scattering experiments on ^{120}Sn are in disagreement with corresponding (p, p') Coulomb excitation data. To examine this discrepancy an additional high-sensitivity bremsstrahlung experiment on ^{120}Sn was performed.

Method: The Nuclear Resonance Fluorescence (NRF) method is used, which is based on the scattering of real photons. The bremsstrahlung experiment presented in this work was performed with a maximum energy of $E_{\gamma,\mathrm{max}} = 9.5$ MeV at the γELBE facility at the Helmholtz-Zentrum Dresden-Rossendorf (HZDR). Besides a state-to-state analysis, the quasicontinuum was investigated as well.

Results: Above $E_x = 4$ MeV 228 dipole transitions were clearly identified; 163 were observed for the first time. Assuming that all identified dipole transitions have electric dipole character the summed electric dipole strength equals $\sum B(E1)\uparrow = 369(49) \times 10^{-3}\ e^2\mathrm{fm}^2$ [which amounts to 0.58(8)% of the Thomas-Reiche-Kuhn sum rule] for transitions from 4 MeV to $S_n = 9.1$ MeV. This is an enhancement of a factor 2.3 compared to the previously published ^{120}Sn(γ, γ') results. This increase can be explained by the contribution of many weak, previously not included transitions in the state-to-state analysis. The photoabsorption cross sections deduced from the quasicontinuum analysis exceed those of the (p, p') experiment in average by about 50% between 5.9 and 8.7 MeV.

Conclusion: The newly extracted summed $B(E1)$ value of the state-to-state analysis is larger than those of ^{112,116}Sn and smaller than that of ^{124}Sn. The difference between the electric dipole transition strengths deduced from isolated peaks of the present (γ, γ') data and those from the inelastic proton scattering experiment above 6.3 MeV is still striking. The analysis of the photoabsorption cross section including the quasicontinuum of levels overcomes this problem and the results are in the order of magnitude of the (p, p') data and continue the (γ, n) cross sections at the neutron separation threshold.

DOI: 10.1103/PhysRevC.102.014317

I. INTRODUCTION

Nuclear astrophysics aims for a deeper understanding of different astrophysical objects, e.g., neutron stars, and of nucleosynthesis processes such as the rapid neutron-capture process (r process). The latter one is one requirement for the existence of the heavier, neutron-rich nuclei in the universe. For calculations of reaction rates within the r process, neutron-capture cross sections are an important ingredient. Since the measurement of such is very hard for unstable nuclei, predictions using, among other parameters, the photon strength function (PSF) are used [1–4]. The PSF of a nucleus describes average transition probabilities in dependence on the involved γ-ray energies. Therefore, the PSF is directly

*muescher@ikp.uni-koeln.de

†Present address: Physikalisch-Technische Bundesanstalt, 38116 Braunschweig, Germany.

‡Present address: Vocational School, Istanbul Kultur University, Incirli Campus, Istanbul, Turkey.

related to the photoabsorption cross section σ_γ. The appearance of additional electric dipole strength like the Pygmy Dipole Resonance (PDR) [5] on top of the low-lying tail of the isovector Giant Dipole Resonance (GDR) influences the reaction rates of the *r* process [1,3,4].

Moreover, if the PDR is imagined in a simplified macroscopic picture as an oscillation of excess neutrons against an isospin-saturated core, the strength of the PDR should be related to the neutron-skin thickness. In turn, the thickness may be used as a constraint on the density dependence of the nuclear Equation of State (EoS) and may lead to a better understanding of, e.g., neutron stars [6,7].

During the last decades, many real photon scattering experiments have been performed to study the low-lying dipole response in atomic nuclei in a model-independent way. The neutron magic $N = 50$ [8–11] and $N = 82$ [12–18] isotonic chains, the $A \approx 50$ [19–26] region, and the $Z = 42$ [27–29], $Z = 54$ [12,30,31], and $Z = 82$ [32–35] isotopic chains were already measured extensively in (γ, γ') experiments. The tin isotopic chain is well suited for systematic studies due to its magic proton number ($Z = 50$) and its many stable, even-even isotopes. This allows a study of the PDR over a wide range of N/Z ratios. Bremsstrahlung experiments have been performed on ^{116,124}Sn by Govaert *et al.* [36] at the linearly bremsstrahlung facility in Gent [37] and ^{124}Sn was measured in a further bremsstrahlung experiment at the Darmstadt High-Intensity Photon Setup (DHIPS) [38] by Schlüter [39,40]. Moreover, bremsstrahlung data of ^{112,120}Sn recorded at DHIPS have already been analyzed by Özel-Tashenov *et al.* [41]. All isotopes were investigated with bremsstrahlung distributions with at least two different endpoint energies to take feeding effects into account. A comparison of the bremsstrahlung results of the tin isotopes shows that the summed strength of ^{120}Sn determined by Özel-Tashenov *et al.* is smaller than that observed in ^{112,116,124}Sn and does not fit the intuitively expected enhancement with increasing neutron excess [41]. However, this could partly be explained by a varying amount of missing strength hidden in weak transitions below the sensitivity limit of the state-to-state analysis, and a contribution by unobserved γ-decay branchings which could not be experimentally extracted in the measurements.

Furthermore, ^{120}Sn has been measured in a (p, p') experiment at the Research Center of Nuclear Physics (RCNP) in Osaka, Japan, by Krumbholz *et al.* [42]. In this experiment nuclei were excited by relativistic Coulomb excitation by proton scattering at high energies ($E_{\text{beam}} = 295$ MeV) and at very forward angles (0°–4°). Therefore, mainly states excited by dipole and quadrupole transitions are populated and it is a well-suited technique to study the complete electric dipole ($E1$) response of atomic nuclei. However, the analysis is not model independent and requires a multipole decomposition in order to extract the $E1$ strength [43]. Consequently, a comparison between the results of both approaches is very important. The summed electric dipole transition strength of the ^{120}Sn(p, p') reaction showed a large discrepancy of more than a factor 7 from the existing (γ, γ') data extracted in the state-to-state analysis between 4 and 9 MeV [42]. For an investigation of these discrepancies an additional bremsstrahlung experiment with high sensitivity was performed on ^{120}Sn.

II. METHOD AND EXPERIMENT

A. Method

1. State-to-state analysis

A well-established experimental approach for studying the dipole response is the Nuclear Resonance Fluorescence (NRF) method [44,45]. Photons excite atomic nuclei from their ground state to an excited state. Due to the small angular momentum transfer, predominantly electric and magnetic dipole and, with a much lower probability, electric quadrupole transitions are induced. The photons emitted subsequently during deexcitation are analyzed concerning their angular distributions which yield information about the quantum numbers of the excited state.

The energy-integrated cross section I_S of the excited states can be derived from the number of registered counts A at the corresponding γ-ray energy E_γ according to

$$I_S = \frac{A}{N_T N_\gamma(E_x)\epsilon(E_\gamma)W(\theta)}. \tag{1}$$

Here, N_T is the number of target nuclei, $N_\gamma(E_x)$ denotes the photon flux impinging on the target with the energy needed for the excitation of the corresponding excited nuclear state (E_x), and $\epsilon(E_\gamma)$ is the detector's full-energy efficiency. $W(\theta)$ denotes the angular distribution, which depends on the detector's position relative to the beam axis and the multipolarity of the transition. To assign a multipolarity to a certain deexcitation, the ratio ω of the transition intensities at the different detector positions has to be computed via

$$\omega = \frac{W(90°)}{W(127°)} = \frac{A(90°)}{A(127°)}\frac{\epsilon(E_\gamma, 127°)\tau(127°)}{\epsilon(E_\gamma, 90°)\tau(90°)}, \tag{2}$$

where $W(90°)$ and $W(127°)$ are the angular distributions at scattering angles of $\theta = 90°$ and $\theta = 127°$, respectively. $\tau(90°)$ and $\tau(127°)$ denote the dead time correction of the corresponding detector. These angles are chosen to maximize the difference in ω between a dipole and a quadrupole transition.

In addition, I_S is related to the ground-state decay width Γ_0, the γ-decay branching ratio Γ_f/Γ, and the so-called spin factor $g = (2J + 1)/(2J_0 + 1)$, where J (J_0) is the spin quantum number of the excited state (ground state) [44]:

$$I_S = g\left(\pi\frac{\hbar c}{E_x}\right)^2\frac{\Gamma_0\Gamma_f}{\Gamma}. \tag{3}$$

By using Eq. (3) and the assumption that most of the transitions are ground-state transitions if no branching transition is observed, i.e., $\Gamma_f/\Gamma = 1$, Γ_0 can be extracted. The presumption of elastic transitions only, i.e., direct decays back to the ground state, can be tested in experiments using quasimonoenergetic γ-ray beams where averaged inelastic photoabsorption cross sections can be determined as described in, e.g., Refs. [13,23,26,29,46].

Using unpolarized bremsstrahlung on an unpolarized target and not measuring the polarization in the exit channel, a parity quantum number assignment is not possible. Therefore, it can only be assumed that the emitted γ rays have electric dipole character. This assumption is supported by parity measurements in neighboring nuclei, e.g., ^{116,124}Sn [36]. In

these isotopes electric multipole characters were determined for nearly all dipole transitions for which an assignment was possible [36] and a similar behavior is likely for ^{120}Sn. The electric dipole transition probabilities can be extracted by inserting the ground-state decay width Γ_0 (meV) and the γ-ray energy E_γ (MeV) in

$$B(E1)\uparrow = 9.554 \times 10^{-4} \times g \frac{\Gamma_0}{E_\gamma^3} \quad e^2\mathrm{fm}^2. \tag{4}$$

The arrow pointing upwards means that the relation is valid for an electric dipole excitation from the ground state to an excited state [44].

2. *Analysis of the quasicontinuum*

At higher energies, the spectrum of photons scattered off ^{120}Sn contains a considerable quasicontinuum formed by many weak transitions between excited states in addition to the dominant resolved peaks. This continuum contains, besides the nuclear contribution of interest, background from natural radioactivity, from atomic-scattering processes of the beam in the target, and, in addition, typical structures of the detector response arising from the different interactions of photons with the detector material. During the analysis, these contributions have to be subtracted.

First, a spectrum of the ambient background has to be scaled to the intensities of background transitions such as transitions following the β decay of ^{40}K and ^{208}Tl, which is then subtracted from the measured spectrum. Furthermore, the spectrum has to be corrected for the detector response. Therefore, spectra of monoenergetic γ rays are simulated using GEANT4 [47–49] which are subtracted sequentially starting from the high-energy end of the experimental spectrum. The atomic background produced in the ^{120}Sn target is obtained from a GEANT4 simulation as well using the photon flux, which can be determined as described in Sec. III A. The relevant intensity of the photons resonantly scattered from nuclear states in ^{120}Sn is obtained by subtracting the atomic background from the response-corrected experimental spectrum.

The remaining intensity distribution contains, besides ground-state transitions (elastic transitions), branching transitions to lower-lying excited states (inelastic transitions) as well as transitions from those states to the ground state (cascade transitions). Since only the intensities of the ground-state transitions are needed for the determination of the photoabsorption cross section, contributions of inelastic and cascade transitions are subtracted from the spectrum. Statistical methods can be applied to estimate the intensities of branching transitions to low-lying excited levels and of the γ-decay branching ratios of the ground-state transitions. The intensities of the ground-state transitions are divided by the corresponding ground-state decay-branching ratios which results in the photoabsorption cross section. This method is a well-established technique and was also applied in earlier photon-scattering experiments at γELBE [11,28,30,50–52].

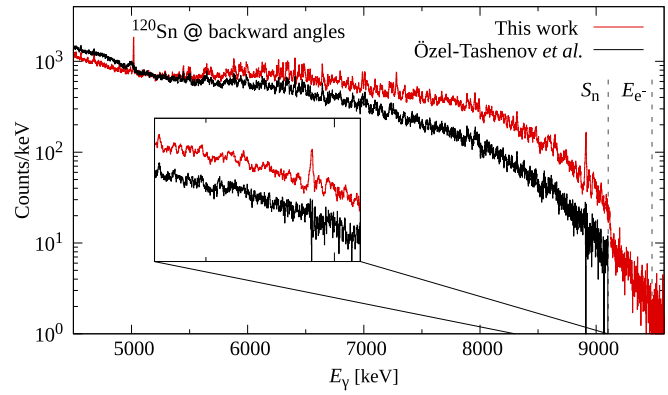

FIG. 1. Comparison of the deexcitation spectra for the detectors at backward angles of the present analysis (red) and the experiment of Özel-Tashenov *et al.* (black) [41]. The black dashed lines mark the neutron separation energy of ^{120}Sn ($S_n = 9.1$ MeV), which was also the endpoint energy of the previous measurement, and the endpoint energy of the new experiment ($E_{e^-} = 9.5$ MeV). The spectra are plotted logarithmically and the inset displays the energy region between 8.3 and 9.1 MeV to illustrate the advantage of using a higher endpoint energy.

B. Experimental details

The bremsstrahlung experiment on ^{120}Sn was performed at the γELBE facility at the Helmholtz-Zentrum Dresden-Rossendorf (HZDR) [53]. The target was irradiated for roughly 130 hours with bremsstrahlung with $E_{\gamma,\mathrm{max}} = 9.5$ MeV. The deexciting photons were detected with four high-purity germanium (HPGe) detectors with a full-energy efficiency of 100% relative to a NaI detector of 7.6 cm diameter and 7.6 cm length at scattering angles of 90° and 127°, two of them at both angles. Each detector was surrounded by a Compton-suppression bismuth-germanate (BGO) shield. Figure 1 illustrates the sum of the deexcitation spectra of both detectors at backward angles (higher statistics, red) and, for a comparison, the spectrum previously measured by Özel-Tashenov *et al.* of one detector positioned at roughly the same angle is displayed (lower statistics, black) [41]. The previous experiment was performed using two different endpoint energies of 7.5 and 9.1 MeV. This enabled the investigation of feeding effects for transitions below 7 MeV by comparing the extracted $B(E1)\uparrow$ values of both measurements. In the analysis by Özel-Tashenov *et al.* no fed states were observed with the exception of the two-phonon 1^- state at $E_x = 3279$ keV [41]. For the present experiment the endpoint energy was $E_{\gamma,\mathrm{max}} = 9.5$ MeV, which is about 0.4 MeV above the neutron separation threshold of ^{120}Sn ($S_n = 9.1$ MeV). This significantly improves the statistics for excitations close to this threshold because of a higher photon flux at these energies. This advantage is depicted in the inset of Fig. 1.

Overall, the statistics and peak-to-background ratios of all transitions are enhanced in the present experiment due to the use of two detectors at each scattering angle instead of one and Compton-suppressing BGO shields. An additional reason may be that the tin target mass (6.488 g) was more than three times higher than in the previous measurement (2 g) [41]. In both experiments the target material was highly enriched

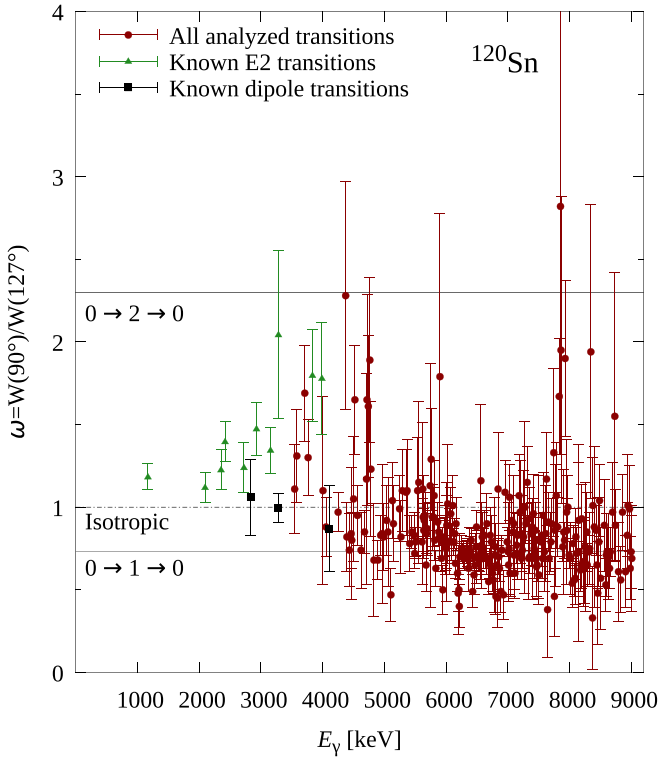

FIG. 2. The intensity ratios ω are depicted in dependence on the γ-ray energy. The green triangles (black squares) show the ratios of previously identified $E2$ (dipole) transitions (see Ref. [54]) which were also observed in this analysis. In addition, the red circles represent all other transitions of ^{120}Sn analyzed in the present experiment. The lowest line indicates the expected intensity ratio of a dipole transition ($\omega = 0.73$) and the top line of a quadrupole transition ($\omega = 2.28$). The intensity ratio equals unity for an isotropic distribution (dashed line).

in ^{120}Sn (> 99%). In addition to the target of interest, a ^{11}B target, which weighted 400 mg, was positioned in the beam as calibration standard. Two of the corresponding well-known transitions of ^{11}B at γ-ray energies of 5018 and 8912 keV can be seen as peaks in the red spectrum of Fig. 1.

III. DATA ANALYSIS AND RESULTS

A. State-to-state analysis

The resulting intensity ratios ω for all 264 analyzed transitions stemming from ^{120}Sn are illustrated in Fig. 2. Above 4 MeV 228 dipole and four quadrupole transitions were clearly identified. A firm assignment means that either $\omega = 0.73$ or $\omega = 2.28$ is within the 2σ range of the experimental intensity ratios ω. The multipolarity assignment was not always possible for transitions with γ-ray energies below 4 MeV because the corresponding intensity ratios are close to unity. One reason for this may be that these states are probably fed by higher-lying states leading to a nearly isotropic γ-ray emission. This phenomenon is shown for most of the known $E2$ transitions (green triangles) in Fig. 2 [54].

For the calculation of the energy-integrated cross section I_S according to Eq. (1), the number of photons hitting the target N_γ and the full-energy peak efficiency $\epsilon(E_\gamma)$ have to be known. The shape of the photon flux is given by the so-called Schiff formula [53,55]. Thereby, it has to be considered that an aluminum hardener was positioned behind the radiator target to reduce the background, especially at lower energies. The shapes of the full-energy efficiencies were determined with a ^{226}Ra source and with a GEANT4 simulation. The product of both quantities was scaled to transitions of the ^{11}B standard for which the total transition widths, angular distributions, γ-decay branching ratios, and multipole mixing ratios are well known [56,57]. Afterwards, the energy-integrated cross section I_S can be determined for both scattering angles. To reduce the total uncertainties the error-weighted average of the two I_S values was calculated and used for the analysis.

With Eq. (4) the electric dipole transition strengths of the observed transitions were determined and the results for all firm and possible dipole transitions are summarized in Table I. The uncertainties given for Γ_0^2/Γ and $B(E1)\uparrow$ consider only statistical uncertainties from the peak fitting and the scaling of the product of photon flux and efficiency. A systematic uncertainty of the number of target nuclei and the photon flux and efficiency determination has to be taken into account; it is estimated to be 10% and is not included in the quoted uncertainties given in Table I.

Above $E_x = 4$ MeV, 163 firm and 15 possible $J = 1$ states were observed for the first time. The summed electric dipole strength is 2.3 times higher than the previous result stemming from a less sensitive measurement [41] and amounts now to $\sum B(E1)\uparrow = 369(49) \times 10^{-3}\ e^2\text{fm}^2$. A possible systematic uncertainty due to peaks that may be contaminated by single-escape events equals only 3.0%.

Six transitions of the previous measurement by Özel-Tashenov *et al.* were not clearly identified in the new deexcitation spectra. For instance, the transition at an excitation energy of 8554.9 keV was assigned in the present analysis to the calibration standard ^{11}B and, therefore, it was excluded. Additionally, the discrepancy between the results of both experiments for the transitions at 6430 and 7973 keV can be explained by transitions of the calibration standard that occur at these energies. In the current analysis the contribution of the corresponding transition of ^{11}B was subtracted. Furthermore, for two other deexcitations (at 7543.1 and 7569.2 keV) of Ref. [41] a clear identification in the present spectra was not possible because the peaks at these energies show double-peak structures.

The $B(E1)\uparrow$ strengths deduced from this measurement and from the experiments by Özel-Tashenov *et al.* [41] are illustrated in Fig. 3 for states above $E_x = 4$ MeV. An energy dependent sensitivity limit was determined for the present experiment by investigating the background B in the deexcitation spectra and using Eq. (5) [40]:

$$A \geqslant \frac{1}{p^2} + \sqrt{\frac{1}{4p^4} + \frac{2B}{p^2}} \tag{5}$$

Here, A equals the minimum peak area which can be resolved and p denotes the limiting relative uncertainty of A, which was chosen to be $p = \frac{\Delta A}{A} \leqslant 30\%$ in this analysis. Afterwards, the extracted peak areas A can be converted into electric dipole

TABLE I. The table contains the excitation energies E_x and the deduced spin quantum numbers for firm and possible $J = 1$ states observed in the present experiment. Spin and parity quantum numbers of some states below 4.2 MeV were already known from Ref. [54] and are listed in the table. Furthermore, the product of the ground-state transition width Γ_0 and the γ-decay branching ratio Γ_0/Γ of this work and of the analysis by Özel-Tashenov *et al.* [41] as well as the transition strengths for all possible electric dipole transitions of this experiment are given assuming $\Gamma_0/\Gamma = 1$. A systematic uncertainty of ± 1 keV can be assumed for the excitation energies.

E_x (keV)	J^π	Γ_0^2/Γ (meV) This work	Ref. [41]	$B(E1)\uparrow$ (10^{-3} e^2fm^2)
2835[a]	1^+	21.0(28)		2.6(4)
3279[a]	(1^-)	146(11)	137(14)	11.9(9)
3547[a]	1,2	24(3)		1.52(22)
3582[a]	(1,2)	24(4)		1.50(23)
3765[a]	$1^+, 2^+$	26(3)		1.40(18)
4006	1	31(9)		1.4(4)
4055	1	31(4)		1.35(18)
4109[a]	1^-	20(3)		0.82(14)
4251	1	75(7)	73(10)	2.81(26)
4393	1	26(4)		0.88(13)
4434	1	25(4)		0.82(13)
4463	1	14(3)		0.45(11)
4472	1	35(4)		1.12(14)
4501	1	18(4)		0.55(12)
4564	1	36(5)	36(8)	1.08(14)
4622	1	25(4)		0.71(12)
4678	1	56(6)	52(10)	1.56(16)
4712	1	17(5)		0.46(15)
4719	1,2	26(6)		0.71(16)
4739	1,2	24(4)		0.65(12)
4765	1,2	22(4)		0.57(11)
4783	1,2	18(4)		0.48(10)
4830	1	17(4)		0.43(10)
4896	1	57(6)		1.38(15)
4939	1	60(6)	36(8)	1.42(15)
4965	1	16(4)		0.38(10)
4991	1	35(5)		0.80(12)
5037	1	37(6)		0.83(12)
5057	1	22(5)		0.49(10)
5107	1	38(6)		0.81(12)
5133	1	38(6)		0.81(12)
5147	1	34(6)		0.72(12)
5245	1	45(6)	22(7)	0.89(13)
5268	1	36(6)		0.71(12)
5291	1	51(8)		0.98(15)
5352	1	45(7)	37(13)	0.85(13)
5369[b]	1	32(6)		0.59(11)
5410	1	48(7)	54(13)	0.87(13)
5447	1	115(11)	126(21)	2.04(19)
5481	1	64(8)		1.11(14)
5492	1	116(11)		2.00(19)
5506	1	112(11)		1.92(18)
5538	1,2	34(7)		0.57(11)
5558	1,2	26(7)		0.43(11)
5612[b]	1	36(7)		0.58(12)
5622	1	62(14)		1.00(22)
5628[b]	1	81(15)		1.30(23)
5637	1	100(11)	109(18)	1.60(18)

TABLE I. (*Continued.*)

E_x (keV)	J^π	Γ_0^2/Γ (meV) This work	Ref. [41]	$B(E1)\uparrow$ (10^{-3} e^2fm^2)
5647	1	152(14)	172(23)	2.42(22)
5658	1	90(10)		1.43(16)
5676	1	60(10)		0.93(14)
5684	1	104(12)	78(20)	1.62(18)
5696	1	68(9)	67(17)	1.06(14)
5742	1,2	52(15)		0.78(22)
5758	1,2	57(10)	42(15)	0.86(14)
5778	1,2	58(9)		0.87(13)
5795	1,2	74(10)		1.08(15)
5804	1	66(10)		0.97(14)
5817	1	127(13)	127(25)	1.84(19)
5831[b]	1	107(12)		1.55(17)
5862	1	118(13)		1.68(18)
5881	1	285(22)	280(40)	4.0(3)
5893	1	158(19)	198(26)	2.21(26)
5900	1,2	45(14)		0.63(19)
5927	1	164(15)	165(25)	2.26(21)
5939	1	193(17)	230(44)	2.64(24)
5949	1	127(16)	139(35)	1.73(21)
5971[b]	1	114(13)		1.53(17)
5988	1	191(22)	203(38)	2.55(29)
5995	1	128(22)		1.70(29)
6001	1	97(23)	168(48)	1.3(3)
6010[b]	1	54(10)		0.71(14)
6026[b]	1	41(9)		0.54(12)
6051	1	65(11)		0.84(14)
6076	1	106(13)	82(21)	1.35(17)
6092	1	148(15)	110(24)	1.88(20)
6110	1	94(13)		1.18(16)
6126	1	272(22)	248(35)	3.39(28)
6139	1	232(20)		2.88(25)
6152	1	212(21)	127(23)	2.61(26)
6160	1	128(16)		1.57(20)
6185	1	126(15)		1.53(19)
6195	1	108(15)		1.30(18)
6207	1	77(17)		0.92(20)
6214	1	141(20)		1.68(24)
6224	1	123(16)		1.47(19)
6252	1	263(23)	255(48)	3.09(27)
6267	1	409(31)	350(44)	4.8(4)
6288	1	225(21)	160(31)	2.59(24)
6305	1	325(27)	270(37)	3.7(3)
6331	1	360(29)	363(54)	4.1(3)
6342	1	384(31)	370(50)	4.3(3)
6352	1	340(29)	259(38)	3.8(3)
6365	1	110(16)		1.23(18)
6374	1	149(19)	118(23)	1.65(21)
6395	1	204(20)	240(40)	2.23(22)
6407	1	520(38)	456(55)	5.7(4)
6430	1	131(17)	142(28)	1.41(18)
6442	1	343(29)	299(52)	3.7(3)
6452	1	119(16)		1.27(18)
6468	1	379(30)	375(62)	4.0(3)
6483	1	392(34)	409(67)	4.1(4)
6492	1	300(29)		3.1(3)
6500[b]	1	136(21)		1.42(22)
6520	1	325(28)	186(32)	3.36(29)

TABLE I. (*Continued.*)

E_x (keV)	J^π	Γ_0^2/Γ (meV) This work	Ref. [41]	$B(E1)\uparrow$ (10^{-3} e^2fm^2)
6537	1	306(27)	219(40)	3.14(27)
6556	1	142(22)		1.44(22)
6563	1	74(18)		0.75(18)
6578	1	72(15)		0.73(15)
6586	1	139(19)		1.39(19)
6602	1	162(19)		1.62(19)
6617	1	125(17)		1.23(17)
6643	1	487(38)	438(68)	4.8(4)
6652	1	190(22)		1.85(21)
6662	1	120(17)		1.17(17)
6690	1	192(21)	206(41)	1.84(20)
6704	1	201(21)		1.91(20)
6716	1	123(18)		1.17(17)
6726	1	246(25)	238(55)	2.31(24)
6735	1	147(21)		1.38(20)
6752	1	157(21)		1.46(20)
6761	1	214(23)		1.98(22)
6791	1	86(25)		0.79(23)
6797	1	288(39)		2.6(4)
6806	1	125(18)		1.13(17)
6824	1	130(19)		1.18(18)
6833[b]	1	90(18)		0.81(16)
6842[b]	1	87(17)		0.78(16)
6854	1	179(21)		1.60(19)
6865	1	249(25)		2.21(22)
6888	1	121(19)		1.06(16)
6902	1	286(28)		2.50(24)
6928	1	91(17)		0.78(14)
6955	1	165(22)		1.40(18)
6989	1	462(42)	376(68)	3.9(4)
7004	1	293(53)		2.4(4)
7010	1	434(59)	480(98)	3.6(5)
7021	1	203(33)	216(41)	1.68(27)
7028	1	256(34)	176(35)	2.11(28)
7036	1	176(25)	160(38)	1.45(21)
7062	1	178(22)	164(48)	1.45(18)
7085	1	119(21)		0.96(17)
7095	1	282(54)	242(65)	2.3(4)
7101	1	241(53)		1.9(4)
7113	1	200(24)		1.59(19)
7142	1	297(32)	259(58)	2.34(25)
7151	1	173(25)		1.35(20)
7160	1	265(31)		2.07(24)
7182	1	126(21)		0.98(16)
7199	1	91(19)		0.70(14)
7220	1	377(44)		2.9(3)
7228	1	195(35)		1.48(26)
7236	1	357(41)	495(64)	2.7(3)
7247	1	232(35)		1.75(26)
7255	1	360(43)	465(88)	2.7(3)
7275	1	143(43)		1.1(3)
7292	1	293(32)		2.16(24)
7313	1	173(24)		1.26(18)
7337	1	139(31)		1.01(22)
7345	1	234(34)		1.69(25)
7354	1	332(36)		2.40(26)
7376	1	147(23)		1.05(16)

TABLE I. (*Continued.*)

E_x (keV)	J^π	Γ_0^2/Γ (meV) This work	Ref. [41]	$B(E1)\uparrow$ (10^{-3} e^2fm^2)
7390[b]	1	181(25)		1.29(18)
7404	1	109(23)		0.77(16)
7414	1	155(26)		1.09(18)
7427	1	282(32)		1.97(22)
7438	1	234(31)		1.63(22)
7447[b]	1	219(30)		1.52(21)
7458	1	315(40)	175(33)	2.18(28)
7465	1	179(33)		1.23(23)
7475	1	283(33)		1.94(23)
7494	1	90(25)		0.61(17)
7503	1	234(33)		1.59(22)
7538	1	224(31)		1.50(21)
7547	1	309(36)		2.06(24)
7565	1	328(42)		2.17(28)
7573	1	197(35)		1.30(23)
7594	1	111(23)		0.73(15)
7615	1	199(44)		1.29(28)
7624	1	180(29)	190(40)	1.16(19)
7645	1	70(22)		0.45(14)
7657	1	206(29)		1.31(19)
7671	1	333(37)		2.11(23)
7698	1	188(30)	229(57)	1.18(19)
7709	1	323(40)		2.02(25)
7744	1,2	106(25)		0.65(16)
7757	1	106(31)		0.65(19)
7765	1	206(36)		1.26(22)
7774	1	135(34)		0.82(21)
7786	1	155(30)		0.94(18)
7806	1	218(32)		1.31(19)
7852	1,2	141(26)		0.86(19)
7861	1,2	125(25)		0.75(18)
7889	1	577(53)	312(62)	3.4(3)
7903	1	244(64)		1.4(4)
7918	1	416(44)		2.40(26)
7951	1	255(66)		1.5(4)
7958	1	642(94)	523(93)	3.7(5)
7973	1	456(30)	606(98)	2.58(17)
7993	1	529(51)	237(48)	2.97(28)
8017	1	140(28)		0.78(16)
8043	1	195(31)	120(30)	1.08(17)
8056	1	414(47)		2.27(26)
8077	1	385(45)	258(100)	2.09(24)
8092	1	265(41)		1.44(22)
8101	1	312(44)		1.68(24)
8113	1	227(35)		1.22(19)
8146	1	217(63)		1.2(3)
8153	1	152(48)		0.80(26)
8177	1	266(37)		1.39(20)
8189	1	296(44)		1.54(23)
8198	1	265(42)		1.38(22)
8218	1	222(50)		1.15(26)
8244	1	290(56)		1.49(28)
8251	1	193(49)		0.98(25)
8277	1	200(36)		1.01(18)
8287	1	380(49)		1.91(25)
8317	1	589(63)	498(96)	2.9(3)
8325	1	215(41)		1.07(20)

TABLE I. (*Continued.*)

E_x (keV)	J^π	Γ_0^2/Γ (meV) This work	Ref. [41]	$B(E1)\uparrow$ (10^{-3} e^2fm^2)
8344	1,2	115(32)		0.57(16)
8372	1	198(49)		0.97(24)
8379	1	308(56)		1.50(27)
8399	1	211(69)	450(100)	1.0(3)
8430	1	326(43)		1.56(20)
8445	1	263(38)		1.25(18)
8459	1	91(29)		0.43(14)
8477	1	240(52)	304(80)	1.13(24)
8485	1	367(55)		1.72(26)
8503	1	96(28)		0.45(13)
8563	1	197(40)		0.90(18)
8587	1	306(54)		1.38(24)
8595	1	256(51)		1.16(23)
8607	1	317(47)		1.43(21)
8638	1	188(43)		0.84(19)
8647	1	414(58)		1.84(26)
8661	1	302(44)		1.33(19)
8697	1	172(35)		0.75(15)
8734	1,2	109(35)		0.47(15)
8743	1	318(54)		1.36(23)
8792	1	118(31)		0.50(13)
8826	1	185(38)		0.77(16)
8858	1	253(41)		1.04(17)
8904	1	300(59)		1.22(24)
8936	1	274(45)		1.10(18)
8946	1	203(41)		0.81(16)
8971	1	294(52)		1.17(21)
8980	1	247(48)		0.98(19)
8993	1	224(42)		0.88(17)
9003	1	145(38)		0.57(15)

[a]Spin and parity quantum numbers taken from Ref. [54].
[b]Possible contamination from single-escape events.

transition strengths by using the equations given in Sec. II A 1. The sensitivity limit of the less sensitive detector is shown due to the condition that a transition has to be observed in all detectors to enable a multipolarity assignment.

The figure depicts the advantage of the new experiment with a higher maximum photon energy once again, i.e., many more transitions were observed especially at higher excitation energies. In general, many weaker transitions increase the number of observed levels in the whole excitation energy region. This may be explained by the use of twice as many detectors at each scattering angle equipped with active anti-Compton BGO shields and by the three times higher target mass during this experiment compared to the measurement by Özel-Tashenov *et al.* [41]. However, when using such a high target mass effects of self-absorption and atomic attenuation within the target itself have to be investigated [58–60]. This means that the photon flux decreases along the target length and is overestimated by the assumption of a constant photon flux distribution impinging on all target nuclei. To test if self-absorption and atomic attenuation have to be considered, the ratios of the $B(E1)\uparrow$ values of this analysis and the previous one by Özel-Tashenov *et al.* [41] were computed

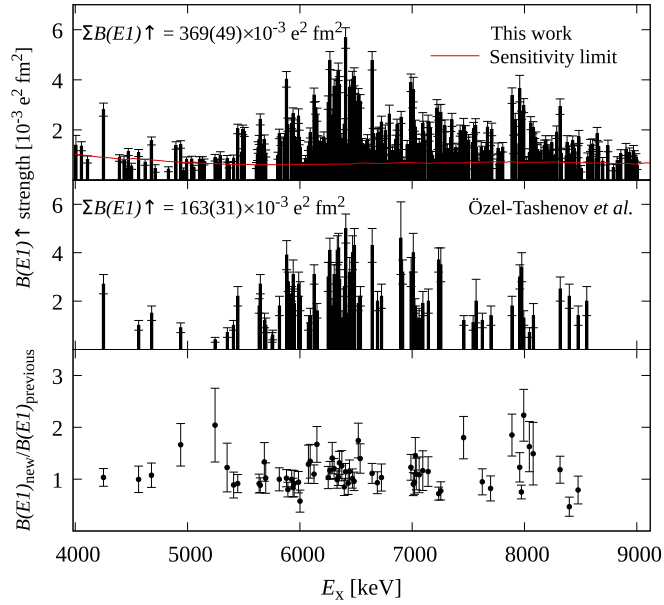

FIG. 3. $E1$ reduced transition strengths obtained in this experiment (top) in comparison to the results determined in the analysis by Özel-Tashenov *et al.* (middle) [41]. Transitions below 4 MeV are neglected because a firm multipolarity determination was not possible. Furthermore, a sensitivity limit was determined for the new analysis and is shown by the red line in the upper panel. In the lower part of the picture the ratios of the above depicted transition strengths are illustrated in dependence on the excitation energy.

and are displayed in dependence on the excitation energy in the lower panel of Fig. 3. Moreover, this ratio was studied as function of the transition strength deduced by Özel-Tashenov *et al.* and dependence on neither the excitation energy nor the transition strength was observed. As a conclusion, the effects of self-absorption and atomic attenuation are negligible within the experimental uncertainties.

Figure 4 illustrates a comparison of the ratios of the extracted summed strengths in ^{112,116,120,124}Sn between 4 and

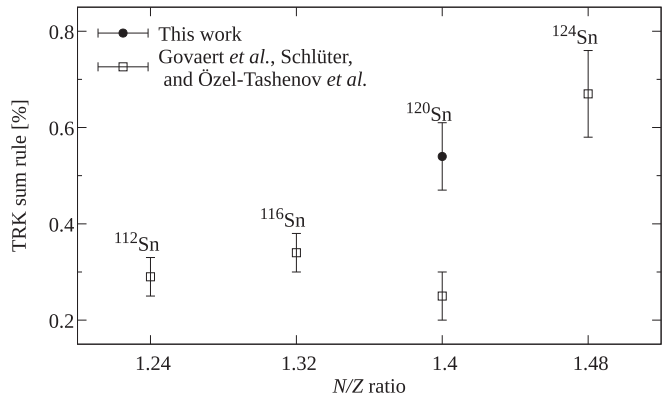

FIG. 4. The figure presents the ratios of the extracted strength in ^{120}Sn of this work (filled circle) and in various tin isotopes already measured in NRF experiments (open squares) [36,39–41] between 4 and 8.5 MeV with respect to the Thomas-Reiche-Kuhn sum rule in dependence on the neutron-to-proton ratio.

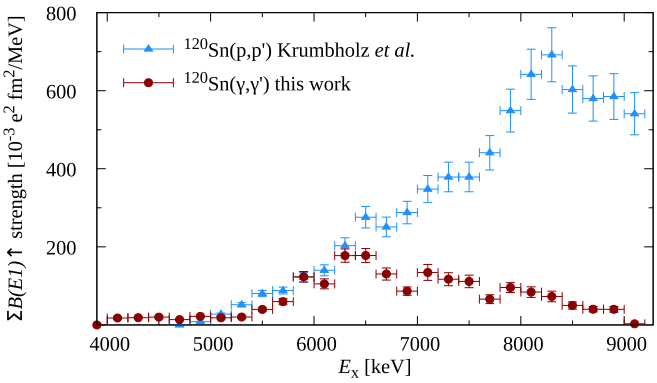

FIG. 5. $\sum B(E1)\uparrow$ values of the isolated states of this NRF experiment (red circles) and of the (p, p') (blue triangles) [42] measurement are displayed in 200 keV bins.

8.5 MeV (S_n of ^{124}Sn) with respect to the Thomas-Reiche-Kuhn (TRK) sum rule in dependence on the neutron-to-proton ratio [61,62]. Within its uncertainty, the newly determined value matches the systematics of an increasing $\sum B(E1)\uparrow$ with an enhancement of the neutron-to-proton ratio. However, it should be emphasized that part of the pygmy strength is located above 8.5 MeV [cf. the (p, p') data in Fig. 4], which may vary depending on the isotope, and that comparisons of different bremsstrahlung experiments may be challenging due to different sensitivity limits. This is shown, e.g., by comparing this new high-sensitivity measurement and the previous experiment by Özel-Tashenov *et al.* (cf. Fig. 3). Furthermore, it has to be taken into account that an electric character is assumed for all dipole transitions with unknown multipole character. However, some of them may be $M1$ transitions whose contribution could be dependent on the isotope.

In addition, Fig. 5 depicts the summed electric dipole strengths in 200 keV bins of the present (γ, γ') experiment (red circles) in comparison to the (p, p') data obtained by Krumbholz *et al.* (blue triangles) [42]. The results up to 6.3 MeV are similar for both probes with the exception of the values at 5.3 and 5.5 MeV. The differences at these energies are probably not explainable by missing strength in the (γ, γ') results due to unobserved γ-decay branching ratios or weak transitions because both effects are not that prominent at low excitation energies. However, these reasons may be explanations for the large discrepancies at energies above 6.3 MeV. Therefore, a measurement with a quasimonoenergetic γ-ray source is very important to compare the results extracted in the analyses using photons and protons. Such experiments can be performed using the Laser-Compton Backscattering technique, e.g., at the High Intensity γ-Ray Source (HIγS) at Duke University [63] and the γ^3 setup [64]. Moreover, this technique provides a linearly polarized photon beam and, therefore, enables the unambiguous determination of parity quantum numbers [65].

B. Analysis of the quasicontinuum

After the correction of the experimental spectrum for the detector response, the efficiency, background radiation, and atomic processes as described in Sec. II A 2, inelastic transitions and cascade transitions have to be removed from the resulting spectrum and the ground-state transitions have to be corrected for their branching ratios b_0. Therefore, γ-ray cascades were simulated from the levels in the whole energy range by using the code γDEX [30,51,52]. γDEX works analogously to the strategy of the code DICEBOX [66] developed for (n, γ) reactions, but in addition it includes the excitation from the ground state. Level schemes ("nuclear realizations") including states with $J = 0$ to 7 were created in these simulations. Experimentally known low-lying levels were included in the simulations. For treating the fluctuations of the partial widths the Porter-Thomas distribution was applied [67].

Level densities were calculated by using the constant-temperature (CT) model [68] with the parameters $T = 0.76(3)$ MeV and $E_0 = 0.12(32)$ MeV adjusted to experimental level densities [69] and, for comparison, by using the back-shifted Fermi gas (BSFG) model with the parameters $a = 13.14(40)$ MeV^{-1} and $E_1 = 0.85(22)$ MeV, also taken from Ref. [69]. The following determination of the absorption cross section is based on the CT level densities. In the individual nuclear realizations, the values of T and E_0 were varied randomly within a Gaussian distribution with a σ corresponding to the uncertainties given in Ref. [69]. The parity distribution of the level densities was modeled according to the information given in Ref. [70]. The starting point $E1$, $M1$, and $E2$ photon strength functions for the simulations were assumed to be Lorentz curves with parameters taken from the RIPL database [71]. The input photon strength functions for the cascade simulations do not affect the results to the same extent as the level densities because they are iteratively modified in the individual steps of the simulations.

The analysis procedure for the determination of the experimental intensity distribution of the ground-state transitions and the branching ratios b_0^Δ in an energy bin $\Delta = 100$ keV is not discussed further in this paper. For more details see, e.g., Ref. [72]. The photoabsorption cross section is obtained from the elastic scattering cross section $\sigma_{\gamma\gamma}^\Delta$ in each bin and for each nuclear realization according to

$$\sigma_\gamma^\Delta = \sigma_{\gamma\gamma}^\Delta / b_0^\Delta. \tag{6}$$

Finally, the deduced photoabsorption cross sections for each nuclear realization were averaged. For the uncertainty a 1σ deviation from the mean has been taken.

The photoabsorption cross sections of ^{120}Sn resulting from the just described procedure using the CT level densities are shown in Fig. 6 (red circles). These cross sections are in average by about 6% greater than the ones obtained by using the BSFG level densities in the γ-ray cascade simulations. The uncertainties caused by using various level-density models were also investigated in Ref. [74]. Based on the results therein and the present differences we estimate an additional systematic uncertainty of up to about 20% for the photoabsorption cross section that is not included in the error bars in Fig. 6. For comparison, cross sections deduced from (γ, n) experiments (gray squares) [73] and from a (p, p') experiment by Krumbholz *et al.* [42] (blue triangles) together with a Lorentz curve using parameters from the

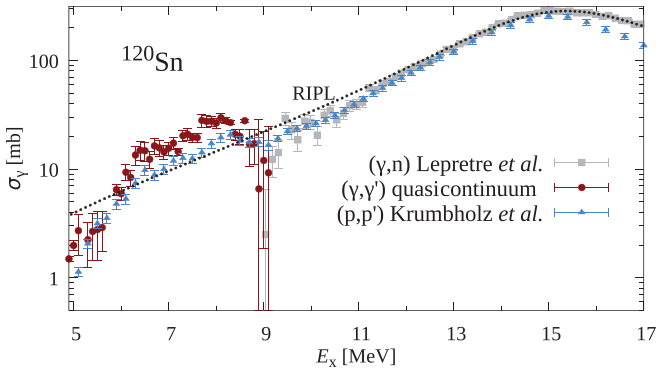

FIG. 6. Photoabsorption cross sections deduced from the analysis of the quasicontinuum of the present measurement (red circles) in comparison with (p, p') data of Ref. [42] (blue triangles) and with (γ, n) data of Ref. [73] (gray squares). Furthermore, a Lorentz curve is illustrated with parameters taken from the RIPL database (black dashed line) [71].

RIPL database (black dashed line) [71] are illustrated. The cross sections extracted in the present analysis continue the (γ, n) cross section toward energies below $S_n = 9.1$ MeV and are in agreement with those around S_n. The photoabsorption cross sections deduced from analyzing the quasicontinuum of the (γ, γ') experiment, however, exceed the (p, p') data in average by about 50% between 5.9 and 8.7 MeV. The relative uncertainties of the extracted values using the CT model below 5.9 and above 8.7 MeV are large and, therefore, the corresponding photoabsorption cross sections were neglected when calculating the averaged difference. This trend is also shown by the contribution to the TRK sum rule in the same energy region as mentioned above, which amounts to 3.1(4)% [2.8(4)%] for the results of the quasicontinuum using the CT model (BSFG model), and to 2.12(3)% for the (p, p') data. For an independent test of the different data sets a (γ, γ') experiment using a quasimonoenergetic γ-ray beam is crucial.

IV. CONCLUSION AND OUTLOOK

In this work the analysis of a new high-sensitivity bremsstrahlung experiment on the proton-magic nucleus ^{120}Sn and the corresponding results are presented.

Above 4 MeV, 228 $J = 1$ states were clearly identified and 163 of these for the first time. Assuming an electric dipole character for these isolated dipole transitions the summed strength equals $\sum B(E1)\uparrow = 369(49) \times 10^{-3}\ e^2\text{fm}^2$. This is an enhancement of a factor 2.3 compared to the results of previous bremsstrahlung measurements performed by Özel-Tashenov *et al.* [41]. This difference may be explained by higher statistics due to more detectors at the two scattering angles, the use of active anti-Compton BGO shields, a higher target mass, and a higher endpoint energy which led to more excitations close to the neutron separation threshold.

With the newly determined $\sum B(E1)\uparrow$ value for ^{120}Sn a systematic comparison of ^{120}Sn with ^{112,116,124}Sn was shown and an increase with increasing neutron excess can be observed for the resolved strength. However, this comparison of bremsstrahlung results for discrete levels just serves as indication of the increasing trend of the summed electric dipole strength and is limited due to different amounts of unresolved strength and γ-decay branching ratios in various nuclei.

Despite the increase of the $\sum B(E1)\uparrow$ value of ^{120}Sn with respect to the previous result [41], it is still more than three times smaller than that of the (p, p') measurement performed by Krumbholz *et al.* [42]. A comparison of the transition strengths in a 200 keV binning shows that this discrepancy is primarily the result of transitions in the excitation region above 6.3 MeV. The deviation may be explained by unobserved γ-decay branchings and unresolved strength. This assumption is supported by the analysis of the quasicontinuum of the bremsstrahlung experiment since the resulting photoabsorption cross sections are comparable to the (p, p') results, which indicates that a considerable amount of strength is hidden in the continuum. However, an averaged difference of about 50% between the present photoabsorption cross sections of the analysis of the continuum and the (p, p') results is observed between 5.9 and 8.7 MeV.

All these deviations can be investigated with a complementary (γ, γ') experiment with a quasimonoenergetic photon beam which provides information about the ratio of γ-decay branching ratios and unresolved strength, as shown in Refs. [29,46]. Furthermore, a measurement with a linearly polarized γ-ray source enables the unambiguous assignment of parity quantum numbers to the corresponding states [65].

ACKNOWLEDGMENTS

The authors thank the accelerator group at the ELBE accelerator for providing an excellent photon beam, the local staff for the help during the experiment, and A. Hartmann for the technical assistance. This work was supported by the BMBF (05P18PKEN9). R.M. acknowledges support by the U.S. Department of Energy, Office of Science, Office of Nuclear Physics under Grant No. LANLE9BW/LANLEM77. J.I. and D.Sy. are supported by the Deutsche Forschungsgemeinschaft (DFG, German Research Foundation) – Project ID 279384907–SFB 1245 and by the State of Hesse under grant "Nuclear Photonics" within the LOEWE program.

[1] S. Goriely, Phys. Lett. B **436**, 10 (1998).
[2] S. Goriely, E. Khan, and M. Samyn, Nucl. Phys. A **739**, 331 (2004).
[3] E. Litvinova, H. Loens, K. Langanke, G. Martínez-Pinedo, T. Rauscher, P. Ring, F.-K. Thielemann, and V. Tselyaev, Nucl. Phys. A **823**, 26 (2009).
[4] A. Larsen, A. Spyrou, S. Liddick, and M. Guttormsen, Prog. Part. Nucl. Phys. **107**, 69 (2019).
[5] D. Savran, T. Aumann, and A. Zilges, Prog. Part. Nucl. Phys. **70**, 210 (2013).
[6] B. Brown, Phys. Rev. Lett. **85**, 5296 (2000).
[7] J. Piekarewicz, B. K. Agrawal, G. Colò, W. Nazarewicz, N.

Paar, P.-G. Reinhard, X. Roca-Maza, and D. Vretenar, Phys. Rev. C **85**, 041302(R) (2012).
[8] R. Schwengner *et al.*, Phys. Rev. C **76**, 034321 (2007).
[9] N. Benouaret *et al.*, Phys. Rev. C **79**, 014303 (2009).
[10] R. Schwengner *et al.*, Phys. Rev. C **78**, 064314 (2008).
[11] R. Schwengner *et al.*, Phys. Rev. C **87**, 024306 (2013).
[12] D. Savran, M. Fritzsche, J. Hasper, K. Lindenberg, S. Müller, V. Y. Ponomarev, K. Sonnabend, and A. Zilges, Phys. Rev. Lett. **100**, 232501 (2008).
[13] A. P. Tonchev, S. L. Hammond, J. H. Kelley, E. Kwan, H. Lenske, G. Rusev, W. Tornow, and N. Tsoneva, Phys. Rev. Lett. **104**, 072501 (2010).
[14] R.-D. Herzberg *et al.*, Phys. Lett. B **390**, 49 (1997).
[15] B. Löher *et al.*, Phys. Lett. B **756**, 72 (2016).
[16] A. Zilges, S. Volz, M. Babilon, and P. Mohr, Phys. Lett. B **542**, 43 (2002).
[17] S. Volz, N. Tsoneva, M. Babilon, and M. Elvers, Nucl. Phys. A **779**, 1 (2006).
[18] D. Savran *et al.*, Phys. Rev. C **84**, 024326 (2011).
[19] T. Hartmann, J. Enders, P. Mohr, K. Vogt, S. Volz, and A. Zilges, Phys. Rev. Lett. **85**, 274 (2000).
[20] J. Isaak *et al.*, Phys. Rev. C **83**, 034304 (2011).
[21] T. Hartmann, M. Babilon, S. Kamerdzhiev, E. Litvinova, D. Savran, S. Volz, and A. Zilges, Phys. Rev. Lett. **93**, 192501 (2004).
[22] F. Bauwens, J. Bryssinck, D. De Frenne, K. Govaert, L. Govor, M. Hagemann, J. Heyse, E. Jacobs, W. Mondelaers, and V. Y. Ponomarev, Phys. Rev. C **62**, 024302 (2000).
[23] M. Scheck *et al.*, Phys. Rev. C **87**, 051304(R) (2013).
[24] H. Pai *et al.*, Phys. Rev. C **88**, 054316 (2013).
[25] Krishichayan, M. Bhike, W. Tornow, G. Rusev, A. P. Tonchev, N. Tsoneva, and H. Lenske, Phys. Rev. C **91**, 044328 (2015).
[26] J. Wilhelmy *et al.*, Phys. Rev. C **98**, 034315 (2018).
[27] G. Rusev *et al.*, Phys. Rev. C **77**, 064321 (2008).
[28] G. Rusev *et al.*, Phys. Rev. C **79**, 061302(R) (2009).
[29] C. Romig *et al.*, Phys. Rev. C **88**, 044331 (2013).
[30] R. Massarczyk *et al.*, Phys. Rev. Lett. **112**, 072501 (2014).
[31] H. von Garrel *et al.*, Phys. Rev. C **73**, 054315 (2006).
[32] T. Chapuran, R. Vodhanel, and M. K. Brussel, Phys. Rev. C **22**, 1420 (1980).
[33] J. Enders *et al.*, Phys. Lett. B **486**, 279 (2000).
[34] N. Ryezayeva, T. Hartmann, Y. Kalmykov, H. Lenske, P. von Neumann-Cosel, V. Y. Ponomarev, A. Richter, A. Shevchenko, S. Volz, and J. Wambach, Phys. Rev. Lett. **89**, 272502 (2002).
[35] J. Enders *et al.*, Nucl. Phys. A **724**, 243 (2003).
[36] K. Govaert, F. Bauwens, J. Bryssinck, D. De Frenne, E. Jacobs, W. Mondelaers, L. Govor, and V. Y. Ponomarev, Phys. Rev. C **57**, 2229 (1998).
[37] K. Govaert *et al.*, Nucl. Instrum. Methods Phys. Res., Sect. A **337**, 265 (1994).
[38] K. Sonnabend *et al.*, Nucl. Instrum. Methods Phys. Res., Sect. A **640**, 6 (2011).
[39] F. Schlüter (private communication).
[40] J. Endres *et al.*, Phys. Rev. C **85**, 064331 (2012).
[41] B. Özel-Tashenov *et al.*, Phys. Rev. C **90**, 024304 (2014).
[42] A. Krumbholz *et al.*, Phys. Lett. B **744**, 7 (2015).
[43] P. von Neumann-Cosel and A. Tamii, Eur. Phys. J. A **55**, 110 (2019).
[44] U. Kneissl, H. H. Pitz, and A. Zilges, Prog. Part. Nucl. Phys. **37**, 349 (1996).
[45] U. Kneissl, N. Pietralla, and A. Zilges, J. Phys. G: Nucl. Part. Phys. **32**, R217 (2006).
[46] J. Isaak *et al.*, Phys. Lett. B **727**, 361 (2013).
[47] S. Agostinelli *et al.*, Nucl. Instrum. Methods Phys. Res., Sect. A **506**, 250 (2003).
[48] J. Allison *et al.*, IEEE Trans. Nucl. Sci. **53**, 270 (2006).
[49] J. Allison *et al.*, Nucl. Instrum. Methods Phys. Res., Sect. A **835**, 186 (2016).
[50] A. Makinaga *et al.*, Phys. Rev. C **82**, 024314 (2010).
[51] G. Schramm *et al.*, Phys. Rev. C **85**, 014311 (2012).
[52] R. Massarczyk *et al.*, Phys. Rev. C **86**, 014319 (2012).
[53] R. Schwengner *et al.*, Nucl. Instrum. Methods Phys. Res., Sect. A **555**, 211 (2005).
[54] K. Kitao, Y. Tendow, and A. Hashizume, Nucl. Data Sheets **96**, 241 (2002).
[55] L. I. Schiff, Phys. Rev. **83**, 252 (1951).
[56] F. Ajzenberg-Selove, Nucl. Phys. A **506**, 1 (1990).
[57] G. Rusev, A. P. Tonchev, R. Schwengner, C. Sun, W. Tornow, and Y. K. Wu, Phys. Rev. C **79**, 047601 (2009).
[58] F. R. Metzger, Prog. Nucl. Phys. **7**, 53 (1959).
[59] V. K. Rasmussen and C. P. Swann, Phys. Rev. **183**, 918 (1969).
[60] R. Vodhanel, M. K. Brussel, R. Moreh, W. C. Sellyey, and T. E. Chapuran, Phys. Rev. C **29**, 409 (1984).
[61] W. Kuhn, Z. Phys. **33**, 408 (1925).
[62] F. Reiche and W. Thomas, Z. Phys. **34**, 510 (1925).
[63] H. R. Weller, M. W. Ahmed, H. Gao, W. Tornow, Y. K. Wu, M. Gai, and R. Miskimen, Prog. Part. Nucl. Phys. **62**, 257 (2009).
[64] B. Löher *et al.*, Nucl. Instrum. Methods Phys. Res., Sect. A **723**, 136 (2013).
[65] N. Pietralla *et al.*, Phys. Rev. Lett. **88**, 012502 (2001).
[66] F. Bečvář, Nucl. Instrum. Methods Phys. Res., Sect. A **417**, 434 (1998).
[67] C. E. Porter and R. G. Thomas, Phys. Rev. **104**, 483 (1956).
[68] A. Gilbert and A. G. W. Cameron, Can. J. Phys. **43**, 1446 (1965).
[69] T. von Egidy and D. Bucurescu, Phys. Rev. C **72**, 044311 (2005).
[70] S. I. Al-Quraishi, S. M. Grimes, T. N. Massey, and D. A. Resler, Phys. Rev. C **67**, 015803 (2003).
[71] R. Capote *et al.*, Nucl. Data Sheets **110**, 3107 (2009).
[72] R. Massarczyk *et al.*, Phys. Rev. C **92**, 044309 (2015).
[73] A. Leprêtre, H. Beil, R. Bergère, P. Carlos, A. D. Miniac, A. Veyssière, and K. Kernbach, Nucl. Phys. A **219**, 39 (1974).
[74] R. Massarczyk *et al.*, Phys. Rev. C **93**, 014301 (2016).